Developmental Biology 374 (2013) 32–45

Contents lists available at SciVerse ScienceDirect

Developmental Biology

journal homepage: www.elsevier.com/locate/developmentalbiology

# Neural differentiation of fragile X human embryonic stem cells reveals abnormal patterns of development despite successful neurogenesis

Michael Telias [a,b], Menahem Segal [c], Dalit Ben-Yosef [a,b,*]

[a] Stem Cell Research Lab, Racine IVF Unit, Lis Maternity Hospital, Tel-Aviv Sourasky Medical Center, 6 Weizmann St., 64239 Tel-Aviv, Israel
[b] Department of Cell and Developmental Biology Sackler Medical School, Tel-Aviv University, Israel
[c] Department of Neurobiology, The Weizmann Institute of Science, Rehovot, Israel

ARTICLE INFO

*Article history:*
Received 3 October 2012
Received in revised form
24 November 2012
Accepted 28 November 2012
Available online 5 December 2012

*Keywords:*
Neural differentiation
Fragile X syndrome
Human embryonic stem cells
Abnormal development
Intellectual disability

ABSTRACT

Fragile X Syndrome (FXS) is the most common form of inherited intellectual disability, caused by developmentally regulated inactivation of *FMR1*, leading to the absence of its encoded protein FMRP. We have previously shown that undifferentiated Fragile X human Embryonic Stem Cells (FX-hESCs) express FMRP, despite the presence of the full *FMR1* mutation ( > 200 CGG repeats). We describe here, for the first time, in-vitro differentiation of FX-hESCs into neurons progressively inactivating *FMR1*. Abnormal neurogenesis and aberrant gene expression were found already during early stages of differentiation, leading to poor neuronal maturation and high gliogenic development. Human FX neurons fired action potentials but displayed poor spontaneous synaptic activity and lacked reactivity to glutamate. Our dynamic FX-hESCs model can contribute to the understanding of the sequence of developmental events taking place during neurogenesis and how they are altered in FXS individuals, leading to intellectual disability. Furthermore, it may shed light over the striking phenotypic features characterizing FXS in human.



## Introduction

Fragile X Syndrome (FXS) is the most common form of inherited intellectual disability. It is an X-linked trait caused by silencing of the *FMR1* gene and the consequent absence of its protein, Fragile X Mental Retardation Protein (FMRP) (Penagarikano et al., 2007).*FMR1* is inactivated due to a dynamic mutation caused by a CGG-triplet repeat expansion in the 5'-untranslated region of the gene (Verkerk et al., 1991). However, the CGG-expansion by itself is not sufficient to cause *FMR1* inactivation, and in FXS individuals, *FMR1* is down-regulated gradually during embryonic development (Sutcliffe et al., 1992; Wang et al., 2012). Indeed, chorionic villi samples taken from FXS fetuses, lack FMRP only at week 12.5 of pregnancy (Willemsen et al., 2002). Furthermore, in healthy fetuses *FMR1* expression is initially expressed in several tissues, but is restricted to neurons later in development (Abitbol et al., 1993; Bhakar et al., 2012), suggesting a role for FMRP in early neurogenesis. Therefore, the initial stages of brain development in both healthy and FX-embryos take place in the presence of FMRP. However, neurons are continuously generated and synapses are still formed even at later stages of development when FMRP is absent in FXS, leading to intellectual disability (Hagerman and Stafstrom, 2009; Hagerman, 1987; Willemsen et al., 2004). Therefore, studies of early neural development and its correlation with *FMR1* gradual inactivation may shed light on the pathophysiology of FXS and the etiology of intellectual disability.

A number of *FMR1* knock-out (KO) animal models have been generated (D'Hulst and Kooy, 2009; den Broeder et al., 2009; Lim et al., 2005; Mientjes et al., 2006; Wan et al., 2000), but they do not express *FMR1* even at early stage of development (Chen et al., 2010). Human in-vitro models for studying FXS include post-mortem adult neurons (Irwin et al., 2001), adult neural progenitors (Schwartz et al., 2005), or fetal neural progenitor cells (Bhattacharyya et al., 2008; Castren et al., 2005). Such cells show mild differences in their morphology and gene expression from normal human controls (Bhattacharyya et al., 2008), but significant differences from their $fmr1^{-/-}$ mice counterparts (Castren, 2006; Castren et al., 2005). Studies on human FX-dendritic spines are inconsistent with their $fmr1^{-/-}$ mice counterparts (Beckel-Mitchener and Greenough, 2004; Braun and Segal, 2000). Consequently, the phenotypic abnormalities observed during FX neurogenesis vary among the different FXS models available for research.

Human Embryonic Stem Cells (hESCs) are of great importance in biology and medicine, due to their ability to grow indefinitely in culture, while maintaining their potential to differentiate into all cell types in the human body (Reubinoff et al., 2000; Thomson et al., 1998). In addition, hESCs can be used to study developmental

* Corresponding author at: Stem Cell Research Lab, Racine IVF Unit, Lis Maternity Hospital, Tel-Aviv Sourasky Medical Center, 6 Weizmann St., 64239 Tel-Aviv, Israel. Fax: +972 3 6925687.
*E-mail address:* dalitb@tlvmc.gov.il (D. Ben-Yosef).

0012-1606/$ - see front matter © 2012 Elsevier Inc. All rights reserved.
http://dx.doi.org/10.1016/j.ydbio.2012.11.031

processes and study genetic disorders, for which no suitable research model currently exists. We have recently derived male FX-hESC lines, carrying the naturally occurring full FXS mutation, from Pre-implantation Genetic Diagnosis (PGD) affected blastocysts (Eiges et al., 2007; Malcov et al., 2007). Our results demonstrated that pluripotent FX-hESCs express *FMR1*, albeit full expansion of the CGG-repeat region (Eiges et al., 2007). Furthermore, we have demonstrated that *FMR1* inactivation is developmentally regulated in FX-hESCs, as it is in human FXS individuals during pregnancy. Recently, human induced Pluripotent Stem Cell (hiPSC) lines were generated from fibroblasts of FXS individuals (Sheridan et al., 2011; Urbach et al, 2010). Despite successful reprogramming of FX somatic cells, *FMR1* remained inactive and FMRP expression was absent, even at the undifferentiated stage, resembling $fmr1^{-/-}$ models. These data highlight critical differences between hESCs and hiPSCs in modeling FXS.

Given these considerations we here focus on the FX-hESC lines we have recently derived, and exploit this unique cell system, to

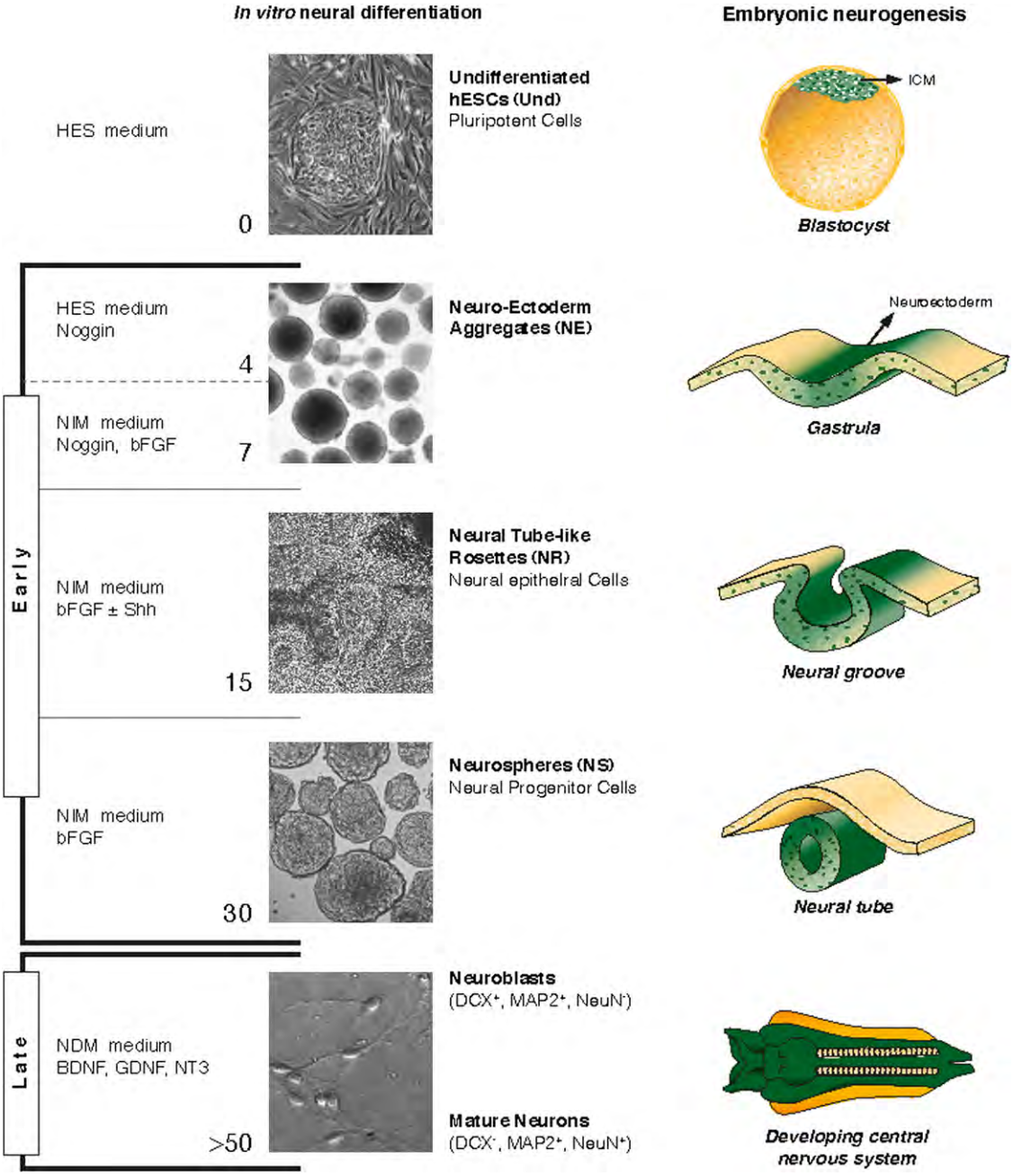


**Fig. 1.** Schematic representation of the in-vitro neural differentiation process. The principal steps of in-vitro neural differentiation are shown in correlation to normal embryonic neurogenesis. Undifferentiated hESCs (Und) are derived from the inner cell mass (ICM) of the blastocyst. Colonies of hESCs are detached and grown in suspension to form aggregates, corresponding to neuro-ectodermal cells (NE) present in the gastrula. Treatment with NIM and noggin was meant to increase the relative amount of neuro-ectoderm in these aggregates. They are then plated onto laminin-coated plates to allow the formation of neural tube-like rosettes (NR) enriched with neuro-epithelial cells. This stage recapitulates neural tube formation with a clear central pseudo-lumen between concentrically elongated neuro-epithelial cells. Fully developed NR are then detached and grown in suspension, allowing them to create neurospheres (NS) enriched with neural progenitor cells, known to be present in the developing central nervous system (CNS) of the embryo. NS are then plated onto poly-D-lysine/laminin-coated coverslips, supplemented with neural differentiation medium (NDM) and pro-neural factors, including BDNF, GDNF and NT-3. Approximately one week following plating, it is possible to observe neuroblasts demonstrating long projections sprouting out from the attached NS. Fully developed neurons are observed approximately $>50$ days following differentiation induction.

describe the sequence of events affecting normal neurogenesis, leading to FXS. In the present study we show for the first time that directed differentiation of FX-hESCs into the neural lineage induced down-regulation of *FMR1* expression, coupled with aberrant expression of key neural genes and phenotypic abnormalities. This is the first report on the successful generation of active neurons from FX-hESCs, which are able to create neuronal networks. The alterations observed during early stages of neurogenesis can explain the abnormalities observed at the end point of the process, including low neurogenic potential and maturation capability, as well as impaired neuronal functionality and poor synaptogenesis. These key differences can probably be attributed mainly to the neuro-developmentally regulated gradual silencing of *FMR1* characterizing both FXS and FX-hESCs.

## Materials and methods

### *Human Embryonic Stem Cells (hESCs)*

The use of spare IVF-derived embryos diagnosed by Pre-implantation Genetic Diagnosis (PGD) for the derivation of hESCs was approved by the Israeli National Ethics Committee (7/04-043). Three male FX-hESC lines were studied: HEFX1 (Ben-Yosef et al., 2011; Eiges et al., 2007; Frumkin et al., 2010), SZ-FX6 (Ben-Yosef et al., 2011) and Lis_FX6 (fully characterized in Fig. 3).In the current study these three lines are entitled FX1, FX2 and FX3, respectively. FX1 and FX3 were established at Tel-Aviv Sourasky Medical Center, while FX2 was kindly provided by Dr. Rachel Eiges from Shaare Zedek Medical Center. Three non-affected *FMR1* hESC lines were used as normal controls: HUES-13, HUES-16 and HUES-6 (Bock et al., 2011; Cowan et al., 2004; Osafune et al., 2008), kindly provided by Dr. Douglas Melton. HUES-13 and 16 are both classified as highly neurogenic lines, while HUES-6 is a low neurogenic line. Cells were cultured on mitomycin-C treated mouse embryonic fibroblasts in hESC medium. Characterization of hESCs included expression of *OCT4*, *NANOG*, *SSEA-3*, *SSEA-4* and *TRA-1-60*. Karyotype analysis was performed as previously described (Eiges et al., 2007). *FMR1* CGG-expansion was analyzed by either Southern Blot as we described previously (Eiges et al., 2007), or by *FMR1* Sizing PCR Kit (Abbott) which is currently used for diagnosing FXS (Fig. S1). Differentiation potential was assessed by teratoma induction, as previously described (Eiges et al., 2007). Teratoma sections were stained with eosin and hematoxylin.

### *In-vitro neural differentiation*

The in-vitro neural differentiation protocol used in this study is based on Xia and Zhang (2009) and Zhang and Zhang (2010) with slight modifications. These protocols, in which undifferentiated hESCs are induced to differentiate into neurons, were designed to mimic the different stages of neurogenesis. In general, the process can be divided into early and late stages of neural differentiation, as depicted in Fig. 1.

*Early stages (day 0 to 30)*

hESC colonies were enzymatically lifted (Collagenase IV, 1 mg/ml) and grown in suspension to create floating Neuro-Ectoderm aggregates (NE). NE aggregates were grown for 7 days: 4 days in DMEM:F12 containing 20% knock-out serum replacement, 1% glutamax, 1% insulin transferrin selenium, 1% non-essential amino acids, 50 ng/ml primocin (InvivoGen) and 200 ng/ml noggin; and 3 days in Neural Induction Medium (NIM) composed of DMEM:F12 containing 1% N2, 0.5% B27 (w/o Vitamin A), 1% glutamax, 1% non-essential amino acids, 50 ng/ml primocin, 20 ng/ml bFGF (R&D) and 200 ng/ml noggin. NE were plated onto laminin (20 μg/ml, Sigma) coated polystyrene well plates (Greiner), and cultured in NIM supplemented with 20 ng/ml bFGF, either alone or with 200 ng/ml Shh (sonic hedgehog), until they developed into neural tube-like rosettes (NR). NR were detached by gentle pipetting and further grown in suspension (NIM supplemented with 20 ng/ml bFGF) to create Neurospheres (NS). Cells still attached to the plate were passaged and stable lines of Neural Precursor Cells (NPCs) were derived.

*Late stage*

At day 30, NS were mechanically triturated, and plated on glass coverslips (Thermo), coated with poly-D-lysine/laminin (Sigma, at a final concentration of 10 μg/ml and 20 μg/ml, respectively). Plated NS were grown in Neural Differentiation Medium (NDM) composed of Neurobasal containing 1% N2, 1% B27 (w/o Vitamin A), 1% glutamax, 1% non-essential amino acids, 50 ng/ml primocin; supplemented with BDNF, GDNF and NT-3 (Peprotech, all at a final concentration of 10 ng/ml). Following NS final plating, neuroblasts developed within one week to 10 days. Full developed neurons and glia were observed $>20$ days post-plating.

### *RNA purification and qRT-PCR*

RNA was extracted (RNeasy Mini Kit – Qiagen), and stored at $-80\,^{\circ}C$, containing RNAse Inhibitor (Roche). DNA decontamination was performed using DNAseI (Roche). RNA (100 ng) was reversed transcribed with Super Script III RT-PCR kit (Invitrogen). Quantitative Real Time PCR (qRT-PCR) was performed using SYBR Green (ABgene). Cycling and analysis were performed using Rotor Gene 6000 Series (Corbett) and its complementary analysis software. The housekeeping gene *GAPDH* was used as a control for ΔΔCt analysis of results. All qRT-PCR assays included Non-Template Control (NTC), non-human control cells (MEF) and adult human-FXS white blood cells. Oligo-DNAs (custom made primers) were purchased from Sigma–Aldrich, see Table S1.

### *Immunostaining*

Cells were fixated with Fixation Buffer (Sigma), incubated overnight at $4\,^{\circ}C$ with primary antibodies in PBS containing 2.5% BSA (Sigma) and 0.5% Triton. Secondary antibodies included sheep α-mouse Cy2-conjugated and goat α-rabbit Cy3- conjugated (Jackson Labs) for 1 h at RT. DAPI (Sigma) was used for nuclear staining in all experiments. Immunostaining was visualized in an Olympus IX51 Inverted Light Microscope or in a Zeiss LSM 510 Confocal Laser Scanning Microscope. Images were processed, including cropping of specific regions of interests, using Olympus CellA or Zeiss LSM Image Browser software, accordingly. For a complete list of all antibodies used see Table S2.

### *FACS analysis*

FACS analysis of undifferentiated hESCs was performed using AF-488 SSEA-3 and AF-647 TRA-1-60 antibodies (BioLegend), and their respective isotype controls. Samples were analyzed using a BD FACS Canto flow cytometer (BD Biosciences).

### *Electrophysiological recordings*

Neurons on glass coverslips were transferred to a recording chamber in standard recording medium, containing (in mM): 10 HEPES, 4 KCl, 2 CaCl2, 1 $MgCl_2$, 139 NaCl, 10 D-glucose (340 mOsm, pH 7.4). Cells were patch-clamped with pipettes containing (in mM) 136 K-gluconate, 10 KCl, 5 NaCl, 10 HEPES,

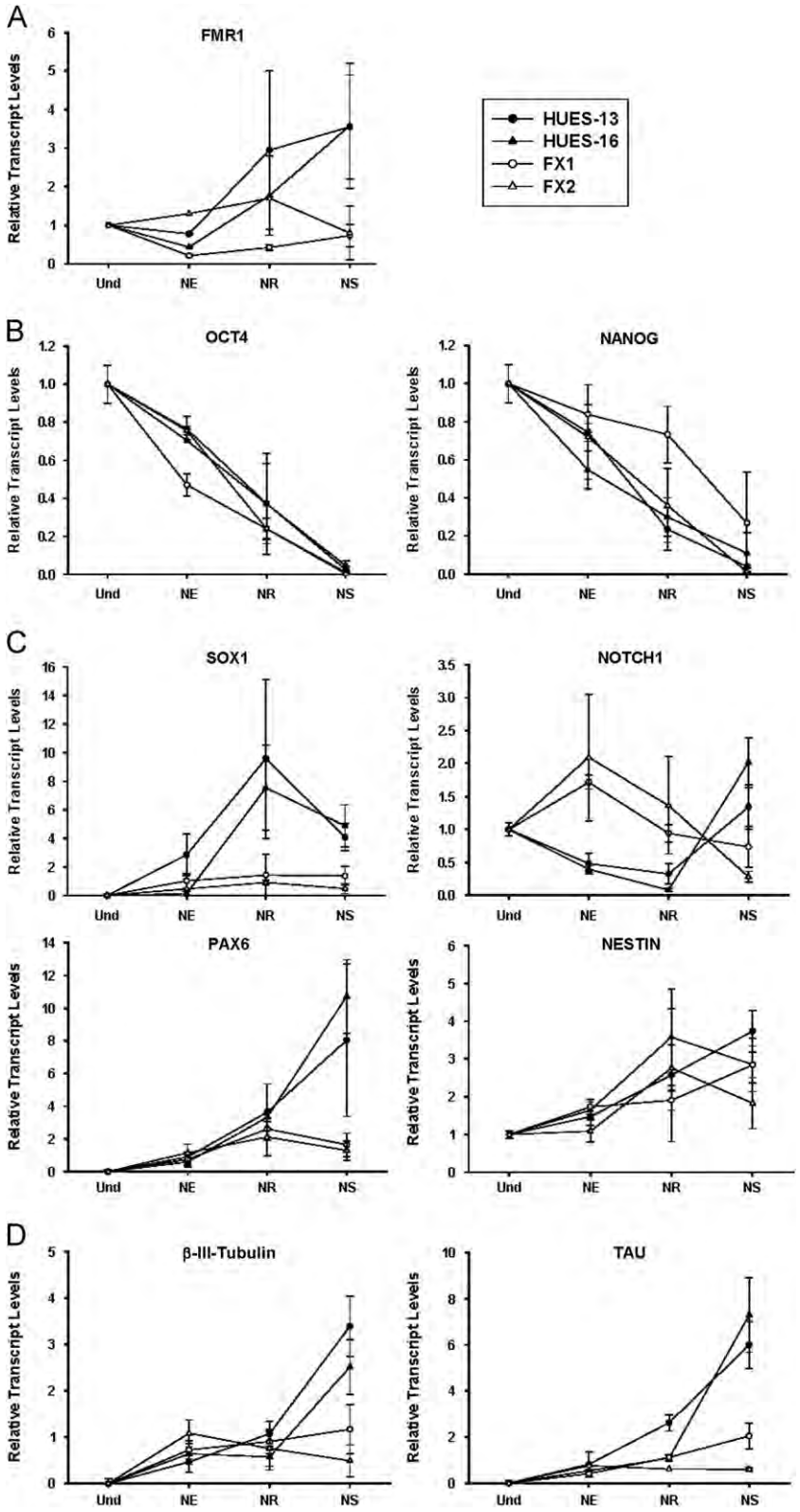


**Fig. 2.** Gene expression analysis of early neural differentiation. Relative transcript levels detected by qRT-PCR in HUES-13 (black circles), HUES-16 (black triangles), FX1 (white circles) and FX2 (white triangles), in 2 or 3 different experiments for each line; calculated as relative to *GAPDH* expression (ΔΔCt) in the undifferentiated sample (mean ± s.e.m.). RNA samples extracted at four time-points along early neural differentiation: Und (undifferentiated, day 0), NE (neuro-ectoderm aggregates, day 7), NR (neural rosettes, day 15–20) and NS (neurospheres, day 30). (A) *FMR1*, (B) Pluripotency markers: *OCT4* and *NANOG*, (C) Early neural genes: *SOX1*, *NOTCH1*, *PAX6* and *NESTIN* and (D) Late neural genes: *β-III-Tubulin* and *TAU* (*MAP-T*).

0.1 EGTA, 0.3 Na-GTP, 1 Mg-ATP, and 5 phosphocreatine, pH 7.2 (pipette tip resistance was 5–8 MΩ). Action potentials were evoked either by injecting depolarizing current pulses (current-clamp) or by depolarizing pulses (voltage-clamp). Membrane potential was held at −60 mV. Spontaneous synaptic currents were recorded continuously for up to 2 min in voltage clamp with

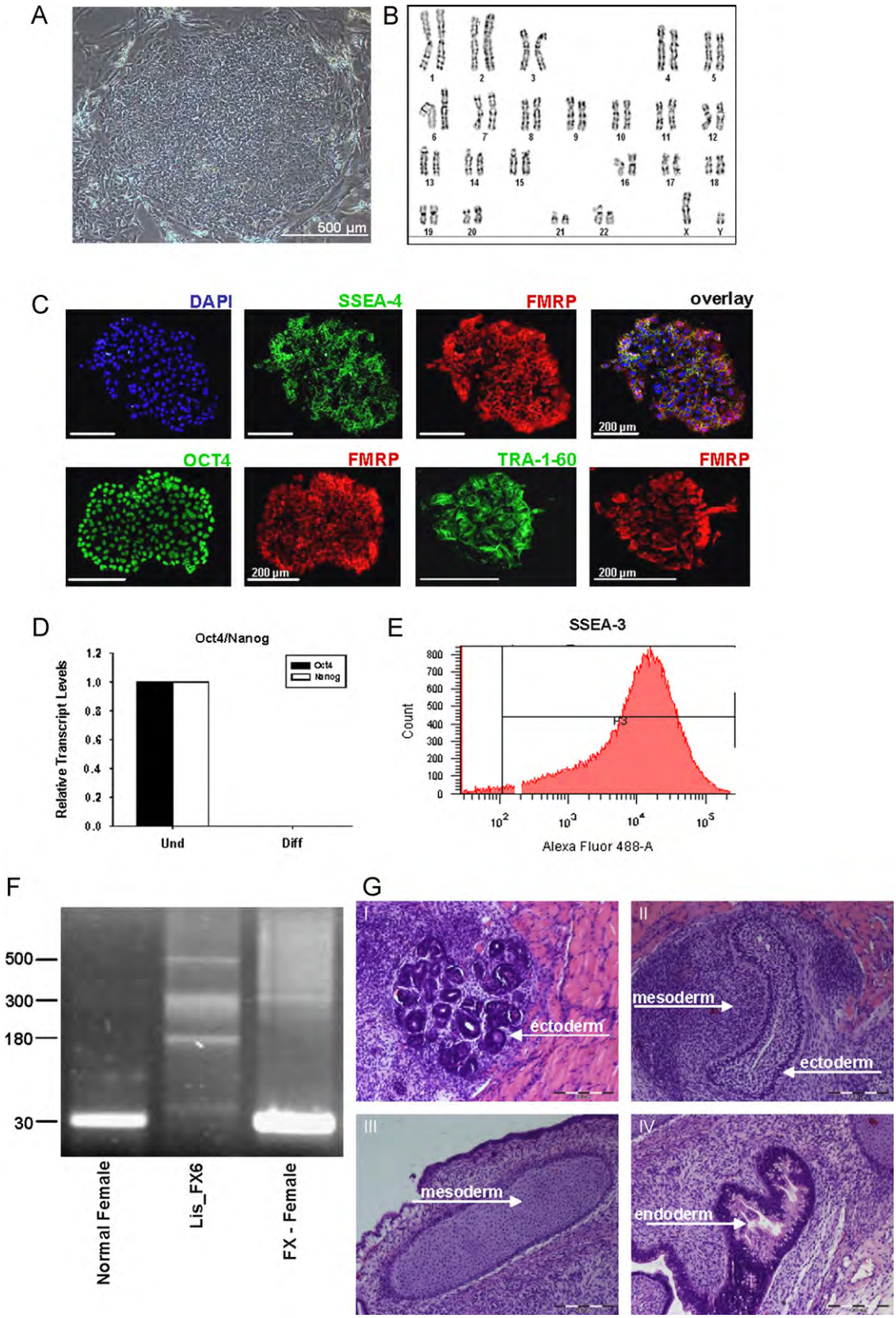


**Fig. 3.** Characterization of Lis_FX6 (FX3) hESC line. (A) Colony morphology of FX3 hESCs at passage 47. (B) Karyotype analysis by Giemsa staining. (C) Immunostaining assays on undifferentiated colonies of FX3 hESC lines for the detection of SSEA-4 (green), FMRP (red), OCT4 (green) and TRA-1-60 (green). Nuclear staining in blue (DAPI). (D) qRT-PCR of *OCT4* (black) and *NANOG* (white) expression in undifferentiated hESCs ("Und") and inactivation following 70 days of differentiation ("Diff"). (E) FACS analysis reveals 89.4% positive cells for SSEA-3. (F) Analysis of *FMR1* CGG repeat expansion, including the full mutation range (180-500 CGG repeats). Normal female and a FX female served as controls. (G) Hematoxylin and eosin staining of FX3-derived teratoma sections, showing tissue structures corresponding to the three germ layers: (I) glandular-like structures (ectoderm), (II) mesenchymal tissue (mesoderm) and epithelial polarized cells (ectoderm), (III) cartilage-like structure (mesoderm); and (IV) intestine-like structure (endoderm).

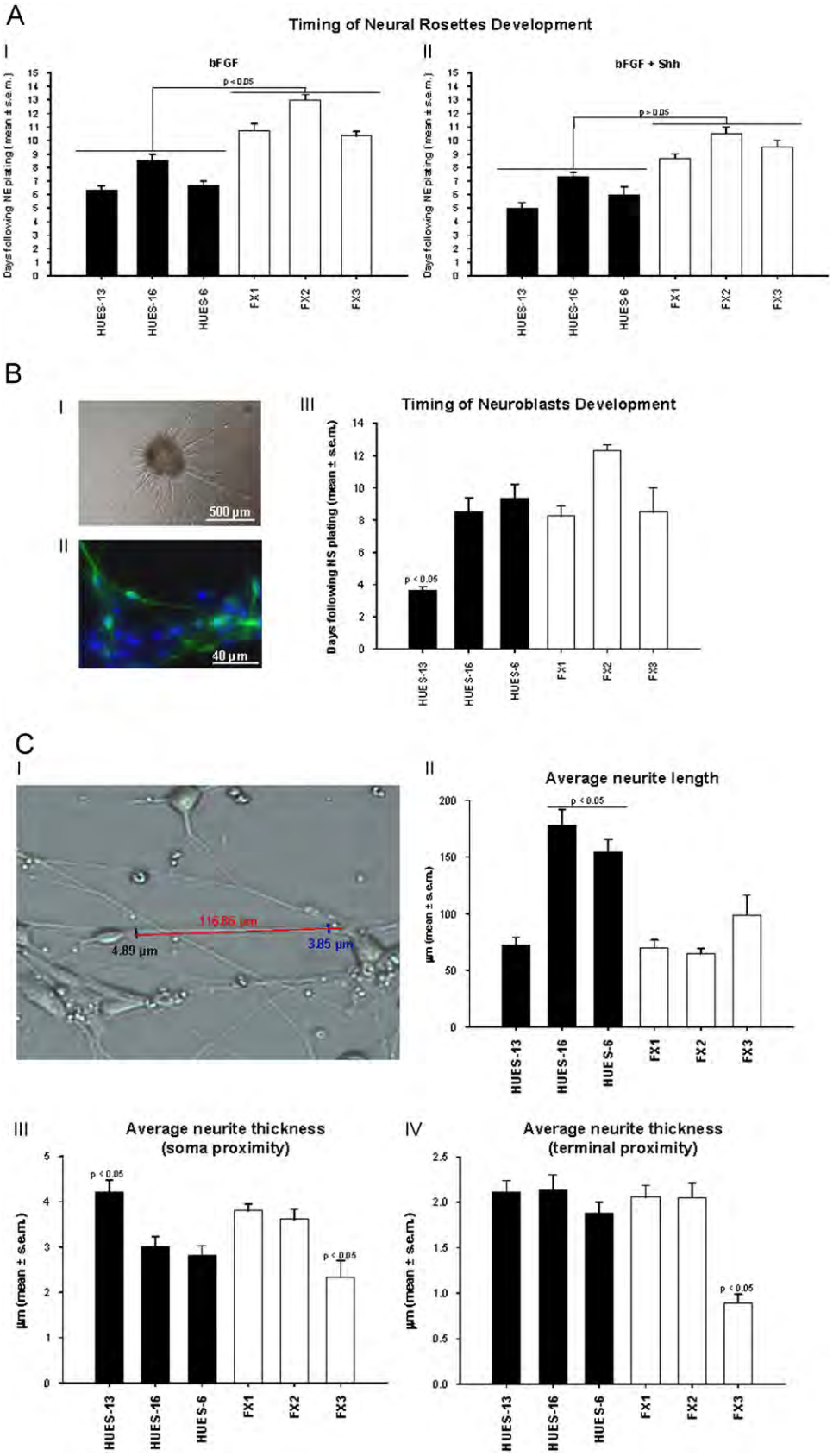


**Fig. 4.** Neural rosettes and neuroblasts development. (A) Neural rosettes (NR) from FX-hESC lines. Timing of NR development: mean number of days ± s.e.m. following plating of neuro-ectoderm aggregates, supplemented with 20 ng/ml bFGF only (I); or together with 200 ng/ml Shh (II). (B) Neuroblasts from FX-hESC lines. A neuroblasts network developing from a single neurosphere 7 days following plating (I). Doublecortin (DCX) immunostaining (green) of neuroblasts (II). Timing of neuroblast development: number of days (mean ± s.e.m.) following neurosphere plating (III). (C) Neurite morphology analysis in neuroblasts, on phase images using the function for arbitrary graphic measurement (from point to point) CellA complementary software – Olympus (I). Neurite length (II), neurite thickness close to the soma (III) and close to the terminal end (IV). Each measurement was performed on at least 40 cells for each line. Values are given in µm (mean ± s.e.m.). Statistical analysis: 1-way ANOVA.

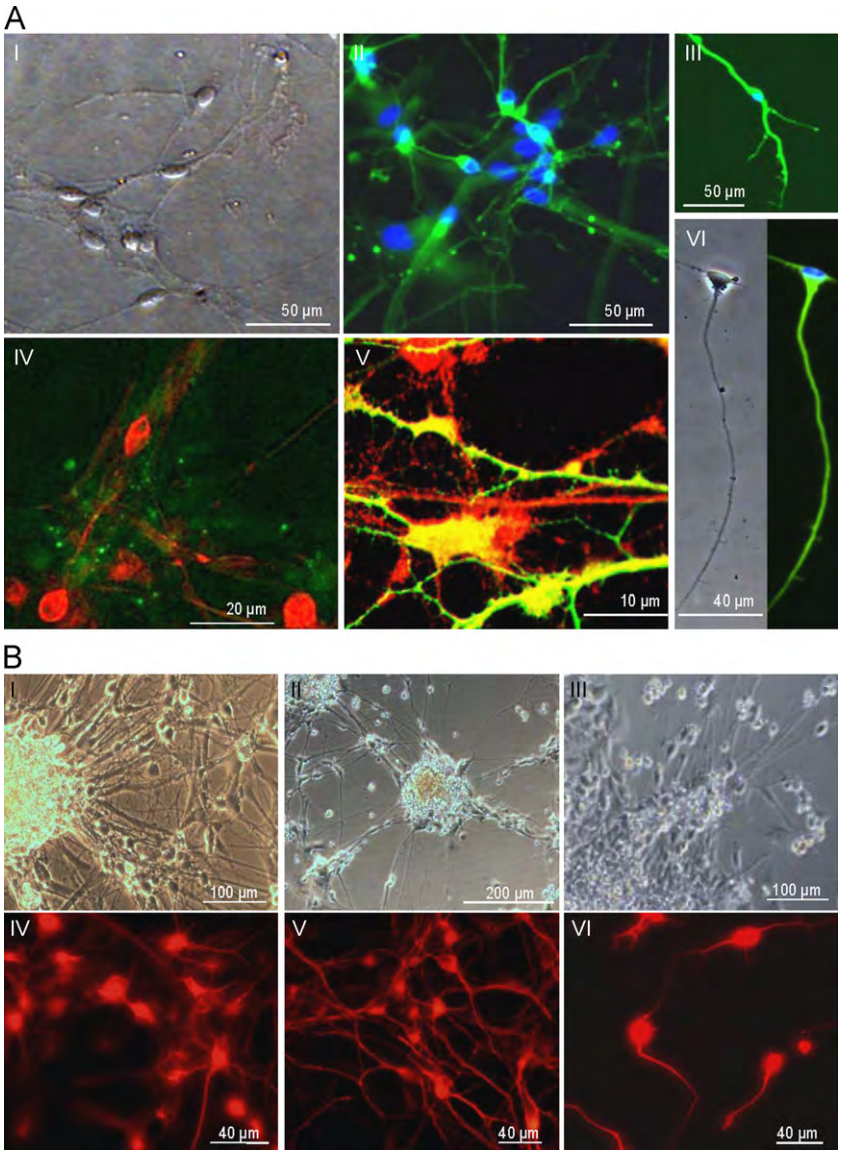


**Fig. 5.** Human FX neurons derived from Fragile X hESCs. (A) Representative pictures of fully developed neurons derived from hESCs. (I) Phase image of an in-vitro neuronal network, (II&III) TUJ1 (β-III-Tubulin) staining (green), (IV) MAP2 (red) and Synaptophysin (green puncta), (V) MAP2 (red) and Synaptotagmin (green puncta), and (VI) bright field (left) and TAU staining (right, green) a single cell. Nuclear staining in blue (DAPI). (B) Representative images of neuronal networks derived from three FX-hESC lines. Bright field images of FX1 (I), FX2 (II) and FX3 (III). MAP2 staining (red) for the same lines (panels V and VI, respectively).

a 50 μs sampling rate. Glutamate was diluted in extracellular recording solution and applied by pressure from a patch pipette. Signals were amplified with a Multiclamp700B amplifier and recorded with Clampex 9.2 software (Axon Instruments). Data were subjected to a 500-Hz low-pass filter and analyzed using Clampfit-9 and SigmaPlot.

## Results

### *Early stages of in-vitro neural differentiation in FX-hESCs*

In the first part of this study we have analyzed the effects of the early stages of neural differentiation (Fig. 1) on two FX-hESC lines (FX1 and FX2), as compared to two control non-affected *FMR1* hESC lines (HUES-13 and HUES-16), by analyzing the expression levels and patterns of several key neural genes, in correlation with *FMR1* expression (Fig. 2). The results demonstrate that neural differentiation induced significant and steady up-regulation of *FMR1* transcription in control lines (Fig. 2A). Following 30 days of differentiation, control neurospheres (NS) demonstrated a ~3.5-fold increase in *FMR1* transcription. In contrast, neural differentiation of FX lines failed to induce any increase in *FMR1* expression. In a previous study we have already demonstrated that FX1 teratoma-derived fibroblasts show a ~20-fold decrease in *FMR1* transcription levels, only after >3 months of culture (Eiges et al., 2007). We therefore hypothesized that even lack of up-regulation following directed neural differentiation of FX cells could be critical for normal neurogenesis. In order to confirm this, we tested the expression pattern and levels of several pluripotent and neural genes in the same model of in-vitro neural differentiation. Our results show that the pluripotency markers *OCT4* and *NANOG* were down-regulated upon induction of in-vitro neural differentiation, in both control and FX cells (Fig. 2B). In contrast, the neural genes *SOX1*, *NOTCH1* and *PAX6* showed aberrant or lower expression in FX1 and FX2, as compared to control counterparts (Fig. 2C). Specifically, *SOX1* and *PAX6* showed lack of activation in FX lines. *NOTCH1* expression

pattern in control lines, showed the expected initial down-regulation followed by later increase as a result of enrichment in neural precursor cells (NPCs) within the NS, as already shown by others (Borghese et al., 2010). However, FX lines showed an aberrant expression pattern of *NOTCH1*, with up-regulation at the neuro-ectoderm (NE) stage and delayed down-regulation, probably linked to the inactivation of *FMR1* in these cells. Nonetheless, other early neural genes such as *NESTIN* (Fig. 2C), *NEUROD1* and *MUSASHI* (data not shown), did not show any significant differences in either expression levels or patterns, between FX and control cells. Late neural genes such as *β-III-Tubulin* and *TAU* (*MAP-T*), which are important for neuronal cytoskeleton formation, can be detected already at early stages, such as neural rosettes (NR) and NS (Fig. 2D). Both genes were significantly up-regulated in control lines (especially in NS) as expected, but were under-expressed in FX lines in correlation with *FMR1* lack of up-regulation. In summary, our results show that, in control hESCs *FMR1* is up-regulated during neural differentiation, correlating with normal neural gene expression. On the other hand, lack of *FMR1* up-regulation in FX lines was concomitant with mis-regulation of key neural genes. These findings were confirmed at the protein level by immunostaining assays performed on FX as compared to control NR (Fig. S2 and Table S3). Altogether these results suggest that *FMR1* may play a substantial role in neurogenesis induction, already at early stages.

### *Neural rosettes and neuroblast development in FX-hESCs*

We have recently derived a new male Fragile X human Embryonic Stem Cell (FX-hESC) line from another PGD patient, entitled Lis_FX6 and named "FX3" in the current study. Full characterization of this new line is shown in Fig. 3. Encouraged by our preliminary results showing abnormal neural gene expression, and following derivation of FX3, we expanded our study to include three FX-hESC lines (FX1, FX2, FX3) and three control lines. Control lines were chosen according to their neurogenic potential: two lines (HUES-13 and HUES-16) are highly neurogenic, and one (HUES-6) is poorly neurogenic (Bock et al., 2011; Osafune et al., 2008). Since FX lines produced NR, albeit under-expression of early neural genes, it was interesting to further analyze structural and phenotypic differences during neurogenesis between FX and control lines. NR developed from both FX and control hESC lines displaying the expected typical morphology (Wilson and Stice, 2006), with a clear central pseudo-lumen surrounded by columnar neuro-epithelium in a circular monolayer structure. However, FX-NR developed significantly slower than control NR (Fig. 4A(I); $p < 0.05$). Addition of the purified neural growth factor Sonic Hedgehog (Shh, 200 ng/ml), known to induce neural tube formation (Christian, 2000), rescued the delay to a non-significant difference in timing of NR development between FX and controls (Fig. 4A(II); $p > 0.05$).

Detachment of NR produced NS. Following NS plating onto PDL/Laminin-coated coverslips, neuroblasts were produced, positively stained for Doublecortin (DCX, Fig. 4B). Neuroblasts developed very early in HUES-13, which was significantly faster than the two other control lines and the three FX lines (Fig. 4B(III)). This is probably related to the intrinsic characteristics of HUES-13 as high neurogenic, and unrelated to *FMR1* expression. Neuroblasts protruded from the attached NS as bipolar cells with a small nucleus usually with two long non-branched neurites that could be measured and compared among the different lines using microscopic imaging and a specialized software (Fig. 4C(I)). Neurite length was significantly longer in HUES-16 and HUES-6 neuroblasts, but similar between HUES-13 and all three FX lines (Fig. 4C(II)). Neurite thickness close to the soma was significantly increased in HUES-13 and significantly decreased in FX3, but non-significantly different among the rest of the lines (Fig. 4C(III)). We have also found that neurite thickness at its terminal end was similar among all lines, besides FX3 (Fig. 4C(IV)). Taken together, these differences cannot account for a role of *FMR1* in neurite formation and elongation, contradicting results published using the drosophila *dfxr*$^{-/-}$ model (Morales et al., 2002) and the murine *fmr1*$^{-/-}$ model (Comery et al., 1997; Guo et al., 2011b; Irwin et al., 2000; Nimchinsky et al., 2001).

### *Biased neuron to glia ratio in FX cells is correlated to FMR1 expression*

During final stages of neural differentiation, at 20 to 30 days after NS plating (50 to 60 days from differentiation induction), fully developed neurons were obtained from all control lines (Fig. 5). These in-vitro hESCs-derived neuronal networks (Fig. 5A(I)) were positively stained for TUJ1, MAP2, TAU and NeuN (Figs. 5A and 6A). These cells also expressed synaptic proteins, including synaptophysin and synaptotagmin (Fig. 5A(III and IV)). Similarly, all three FX lines produced complex neuronal networks, although at lower yield, and these neurons could be kept in culture for several weeks (Fig. 5B). Following this final stage of neuronal differentiation, we examined FMRP expression in $>60$ days old neurons (MAP2$^+$ and NeuN$^+$) and glial cells (GFAP$^+$), developed from both control and FX lines. Control neurons expressed FMRP, similar to what is known from healthy individuals (Fig. 6A(I) and (II), upper panels). However, FX neurons developed in-vitro from FX-hESCs, lacked FMRP (Fig. 6A(I) and (II); lower panels). Interestingly, both control and FX glial cells (GFAP$^+$) expressed FMRP (Fig. 6A(III)). Inactivation of *FMR1* in late stages of neural differentiation of FX lines was confirmed by qRT-PCR in FX NPCs and in mechanically isolated FX neurons (Fig. 6A(V)). These results indicate that: (i) FX-hESCs can successfully differentiate into neurons in-vitro; (ii) this model mimics the process of *FMR1* inactivation as it occurs during embryogenesis of FXS fetuses, with expression of *FMR1* at early stages and it is developmentally regulated by silencing until complete inactivation in FX neurons.

In order to compare the neurogenic potential of FX cells to their control counterparts, we carried out double immunostaining assays for MAP2/GFAP on these cultures (Fig. S3). Quantification of these assays revealed that neuronal yield (MAP2$^+$ cells) of control lines corresponded their neurogenic potential (Bock et al., 2011; Osafune et al., 2008), with the high neurogenic lines HUES-13 and HUES-16 producing $>70\%$ neurons and the low neurogenic line HUES-6 producing $\sim 25\%$ neurons (Fig. 6B(I)).

In contrast, all FX lines produced low neuronal yields, similar to HUES-6. Since HUES-6 actively expresses *FMR1*/FMRP, similar to the other two control lines, we conclude that low neurogenic potential of FX lines is only partially caused by lack of FMRP. Quantification of GFAP$^+$ cells revealed a very low production of glia ($<15\%$) in all three control lines. In contrast, all three FX lines produced $>70\%$ GFAP$^+$ cells (Fig. 6B(II)). In all control lines, there were cells ($\sim 27\%$ to 65%) which did not stain positive for either MAP2 or GFAP (double negative) (see Table S4). This double negative population was significantly reduced in FX1 ($\sim 5\%$) and FX3 ($\sim 11\%$). Moreover, in FX2 line $\sim 19\%$ of cells were stained positive for both MAP2 and GFAP (double positive; Table S4). Since GFAP$^+$ cells in FX1, FX2 and FX3 are still FMRP$^+$ (see Fig. 6A(III)), we conclude that this bias of FX cells towards the glial lineage is linked to the aberrant neurogenesis of FX lines, observed already at early stages, due to abnormal regulation of *FMR1*.

### *Functional analysis of human FX neurons*

In order to increase FX neuronal yield, we seeded the FX NS at a higher density (two- to three-fold higher than standard protocol). Indeed, in these conditions, the yield of FX neuronal cultures increased, allowing us to perform extensive electrophysiological analysis into their functional properties. Neurons obtained from

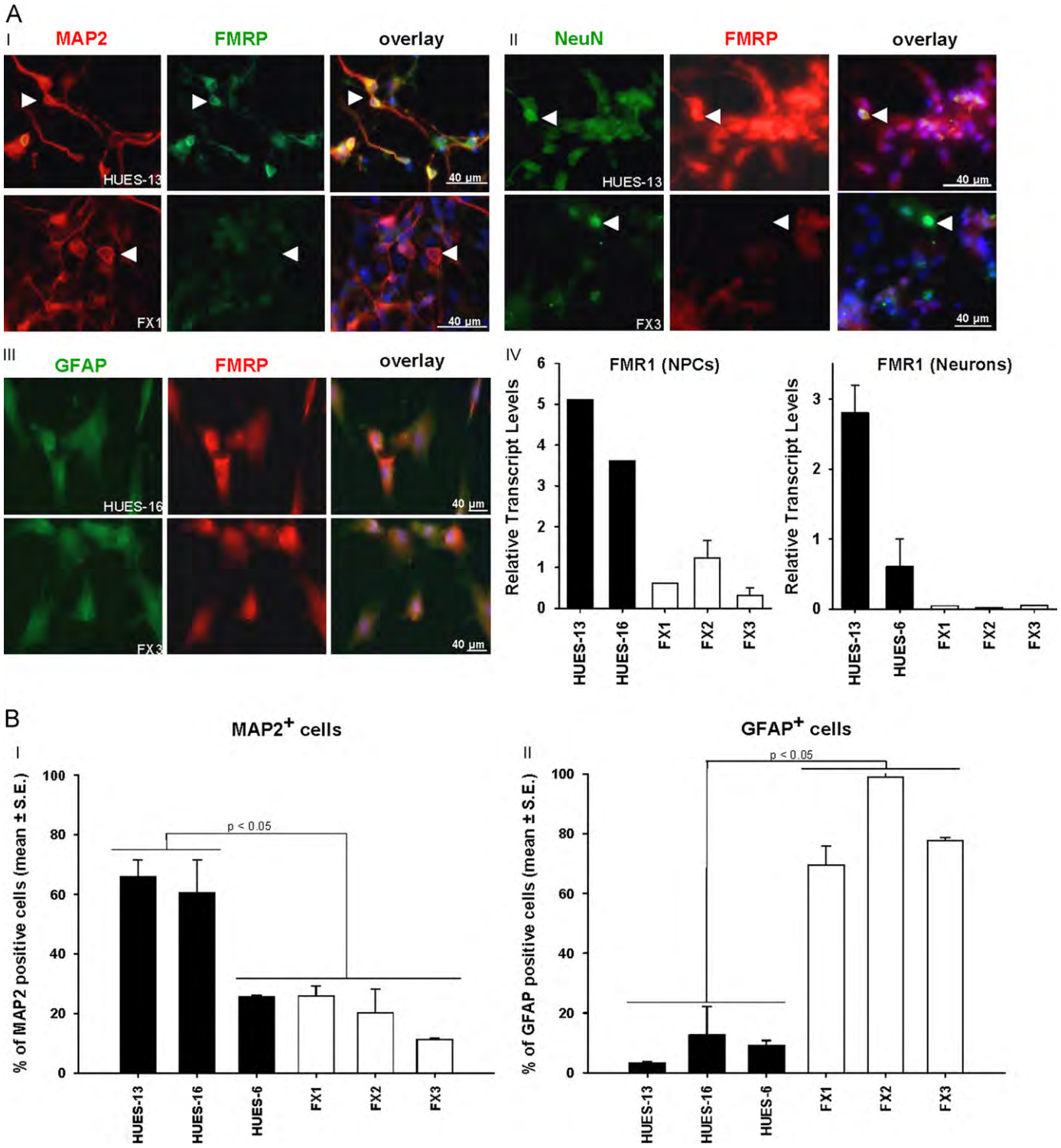


**Fig. 6.** Late neural development of FX and control hESCs. (A) Representative pictures of double immunostaining assays (repeated in all lines). (I) FMRP (green, monoclonal) and MAP2 (red): co-localization in HUES-13 (yellow), but not in FX1. (II) NeuN (green) and FMRP (red, polyclonal): co-localization in HUES-13 (yellow), but not in FX3. (III) FMRP (red) co-localized with GFAP (green) in both HUES-16 and FX3 cells. (IV) *FMR1* relative transcript levels analyzed by qRT-PCR in control and FX neural precursor cells (NPCs, left) and in isolated neurons (right). Each bar represents the level of transcription relative to its undifferentiated stage. (B) Quantification of MAP2 (I) or GFAP (II) stained cells, in at least 5 fields including at least 30 cells per field, for each line studied, for each experiment carried out. Values correspond to average percentage (%) of MAP2 or GFAP positive cells relative to total DAPI staining. Statistical analysis: 1-way ANOVA.

HUES-13 and FX3 lines were selected for electrophysiological analysis, in order to assess both intrinsic and synaptic neuronal properties. Voltage clamp recordings did not reveal significant differences between control and FX neurons; as both expressed inward $Na^+$ currents, and two types of outward $K^+$ currents, a transient and a sustained one (Fig. S4). Current clamp recordings revealed that passive properties (membrane time constant, resting potential and input resistance) are similar in control as

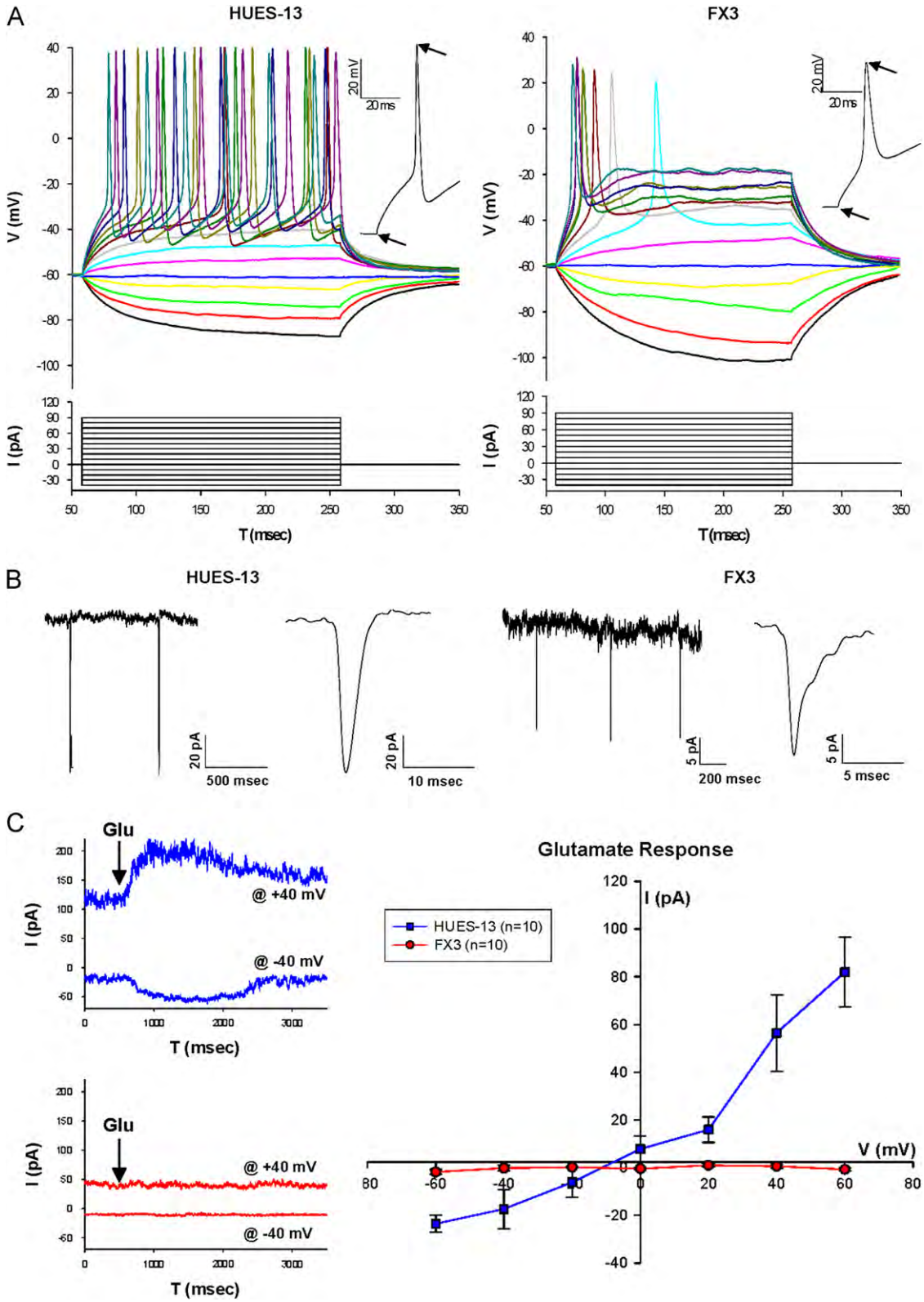


**Fig. 7.** Patch clamp recordings from wt and FX neurons. (A) Representative illustrations of action potentials recorded in current clamp mode. Holding potential was ~ −60 mV. Cells were subjected to 14 consecutive 10 pA current pulses (bottom), and their voltage deflection was recorded (top). Insets (taken from the *I–V* illustrations): first action potential in response to the depolarizing current pulse. Arrows in inserts show the two points for measurement of Spike Rise Time (see Table 1). (B) Representative traces of spontaneous synaptic currents recorded from patch-clamped neurons in voltage clamp mode (left: HUES-13, cell #5 in Table 1B; and right: FX3, cell #1 in Table 1B). (C) Left: representative traces of glutamate response of patch-clamped neurons from HUES-13 (blue) and FX3 (red) at −40mV and +40 mV. Right: *I–V* curve of glutamate response from −60 to +60 mV (mean ± s.e.m.), for HUES-13 (blue, 2 mM glutamate, $n=10$) and FX3 (red, 2 mM glutamate, $n=8$; 200 mM glutamate, $n=2$; total $n=10$).

compared to FX (Fig. 7A and Table 1). However, analysis of action potential properties demonstrated significant differences between FX and control in spike rise time and duration, and in the maximum number of spikes per depolarization (Table 1). The threshold for evoking an action potential was not significantly different, but FX3 neurons expressed a much slower action

**Table 1**
Summary of data obtained from current clamp recordings. Summary of results obtained from recordings in current clamp modality in 20 HUES-13 neurons and 20 FX3 neurons. $\tau$ – time constant of decay obtained from exponential standard fitting curve $f(t)=\Sigma Aie^{-t/\tau i}+C$. Em – Resting membrane potential. Rin – Input resistance. Spike amplitude values above 0 mV. Spike rise time was measured in ms, as depicted by black arrows in the insets of Fig. 7A. Values in the table are given as mean ± s.e.m. *P* values obtained by *t*-test.

| **Current clamp** | **HUES-13** ($n=20$) | **FX3** ($n=20$) | ***p* value** |
|---|---|---|---|
| $\tau$ (msec) | 47.30 ± 5.98 | 42.92 ± 3.33 | 0.53 |
| **Em** (mV) | −60.18 ± 1.63 | −63.52 ± 2.24 | 0.51 |
| **Rin** (MΩ) | 732.63 ± 86.33 | 699.14 ± 52.50 | 0.74 |
| **Max. spikes per depolarization** | 2.75 ± 0.43 | 1.00 ± 0.00 | < 0.001 |
| **Spike threshold** (mV) | −24.78 ± 1.70 | −19.75 ± 1.97 | 0.10 |
| **Spike amplitude** (mV) | 25.64 ± 2.86 | 25.05 ± 2.48 | 0.88 |
| **Spike rise time** (ms) | 27.79 ± 3.74 | 13.36 ± 1.06 | < 0.001 |
| **Spike duration** (ms) | 2.83 ± 0.25 | 3.83 ± 0.28 | 0.02 |
| **After potential** (mV) | −4.51 ± 2.90 | −4.49 ± 1.70 | 0.26 |

**Table 2**
Summary of recorded spontaneous synaptic currents in voltage clamp. HUES-13 and FX3 neurons were analyzed in voltage clamp modality for their capability of spontaneously generating synaptic currents (5 out of 10 HUES-13 neurons and 2 out of 10 FX3 neurons). Measured parameters in each cell included: total number of Synaptic Currents observed during 2 min of continuous recording, Rise Time, Amplitude and $\tau$ (time constant of decay, obtained from exponential standard fitting curve $f(t)=\Sigma Aie^{-t/\tau i}+C$). All values in the table are given as mean ± s.e.m.

| Synaptic currents | **Cell #** | **Synaptic currents** | **Rise time (msec)** | **Amplitude (pA)** | **$\tau$ (ms)** |
|---|---|---|---|---|---|
| **HUES-13** | 1 | 14 | 2.49 ± 0.20 | −19.77 ± 1.29 | 5.93 ± 1.84 |
| (5 out of 10) | 2 | 7 | 1.64 ± 0.07 | −21.06 ± 3.34 | 3.43 ± 0.55 |
| | 3 | 10 | 1.67 ± 0.15 | −26.01 ± 3.05 | 2.02 ± 0.22 |
| | 4 | 50 | 2.03 ± 0.05 | −98.19 ± 1.27 | 2.32 ± 0.04 |
| | 5 | 2 | 2.25 ± 0.25 | −114.80 ± 36.34 | 2.57 ± 0.08 |
| **FX3** | 1 | 20 | 1.23 ± 0.07 | −21.62 ± 0.42 | 1.18 ± 0.14 |
| (2 out of 10) | 2 | 12 | 1.57 ± 0.37 | −16.10 ± 0.92 | 0.94 ± 0.45 |

potential, which was not followed by spike after hyperpolarization, as was in HUES-13 neurons (see Fig. 7A, insets; and Table 1). In voltage clamp recording mode we analyzed the occurrence and characteristics of spontaneous synaptic currents (Fig. 7B). In 5 out of 10 control neurons tested, spontaneous synaptic currents were detected. In contrast, only 2 of 10 FX3 neurons expressed synaptic currents. FX3 synaptic currents displayed lower values of rise time and time constant of decay ($\tau$), but almost similar values of amplitude, as compared to HUES-13 (Table 2). Finally, we assessed whether these hESCs-derived neurons were responsive to glutamate. Representative traces show that control neurons responded to glutamate, at holding potential of −40 mV by a reversible inward current, and at holding potential of +40 mV by an outward current (Fig. 7C, blue). *I–V* curve of glutamate responses shows that in HUES-13 neurons the response to glutamate reversed around 0 mV. Interestingly, even the two FX3 neurons that expressed synaptic currents were unresponsive to glutamate, at any voltage tested, even with glutamate concentrations that were 100-fold higher than those used for control (Fig. 7C, red). It is also important to mention that all FX3 neurons tested for glutamate responses were found to be electrically excitable (by both current and voltage clamp), before and after glutamate application. These results demonstrate that FX-hESC cells can differentiate into viable neurons, which display passive properties similar to control cells. However, FX3 neurons hardly developed functional synaptic connections.

## Discussion

In the present study we have used a dynamic Fragile X human Embryonic Stem Cells (FX-hESCs) model in order to analyze the temporal sequence of events during neural differentiation. This is the only research model of Fragile X Syndrome (FXS) that recapitulates neurogenesis in a human system in which *FMR1* is expressed at early embryogenesis and is developmentally inactivated, similar to the process occurring in human FX fetuses. The results of the current study show that direct differentiation into the neural lineage induces gradual down-regulation of *FMR1* expression in FX-hESCs, as opposed to the *FMR1* up-regulation characterizing this stage in control counterparts. Early stages of FX neurogenesis show aberrant expression patterns of key neural genes and developmental abnormalities in neural rosettes (NR). During final stages of neural differentiation, a significant shift towards the glial lineage was observed in FX lines, in correlation with *FMR1* expression. Albeit the abnormalities observed in FX cells during the process, and their low neuronal efficiency, these are the first human FX pluripotent cells that developed into electrophysiologically active neurons. Extensive functional analysis of these neurons shows that *FMR1* down-regulation leads to the formation of neurons with poor synaptic capability and lack of response to glutamate.

*FMR1* expression was already shown to be restricted mainly to the central nervous system during human embryogenesis (Abitbol et al., 1993), and its absence was shown to be coupled with abnormal neurogenesis (Castren, 2006; D'Hulst and Kooy, 2009). However, the spatiotemporal sequence of events linking between gradual down-regulation of *FMR1* and abnormal neurogenesis are difficult to observe in KO animal models, since *FMR1* expression is absent in these animals even at early stages of development. We have previously demonstrated that FX-hESCs recapitulate in-vivo FXS pathology, by expressing in-vitro *FMR1*/FMRP at the undifferentiated pluripotent stage, which is gradually down-regulated along spontaneous differentiation (Eiges et al., 2007). We show here that directed differentiation into the neural lineage is characterized by lack of *FMR1* up-regulation, concomitantly with an aberrant expression pattern of *SOX1*, *PAX6* and *NOTCH1*, genes that have been found to be responsible for inducing neurogenesis (Borghese et al., 2010; Chambers et al., 2009; Georgala et al., 2011; Yan et al., 2009). In contrast, other neural genes such as *NESTIN* showed normal activation in FX-hESC lines. In accordance, neural progenitors differentiated from FX human induced Pluripotent Stem Cells (hiPSCs) showed a significant reduced expression of *SOX1*, but a normal expression of *NESTIN* (Sheridan et al., 2011). In human FX neural progenitors, harvested from a FXS fetus (with inactive *FMR1*), neural differentiation resulted in the abnormal expression of several neurodevelopmental genes (Bhattacharyya et al., 2008). Since FMRP is an mRNA-binding protein controlling levels of translation, subtle dosage alterations could be responsible for important genetic mis-regulation.

In the present study, we show that aberrant expression of *SOX1* and *NOTCH1* in FX lines was observed in parallel with a significant delay in FX neural rosettes (NR) development. This delay was rescued by addition of soluble sonic hedgehog (Shh), a morphogen which plays a key role in regulation of organogenesis, including brain development. It is tempting to speculate that lack of *FMR1* up-regulation in FX lines is probably sufficient to induce delayed NR formation. Rescue of NR formation by Shh, as well as aberrant expression of *SOX1* and *NOTCH1* in the FX cells, both suggest that *FMR1* is probably involved in the Wnt signaling pathway, affecting several aspects of neural differentiation (Christian, 2000; Guo et al., 2011b; Kormish et al., 2010; Luo et al., 2010; Patapoutian and Reichardt, 2000; Shih et al., 2010)

Furthermore, it was demonstrated that the interaction between *FMR1*/FMRP with members of the Wnt signaling pathway is critical for adult neurogenesis in the murine hippocampus (Guo et al., 2011b; Luo et al., 2010).The current study further demonstrates such a link, between FMRP and Wnt, at early stages of neural development.

FX neuroblasts developed neurites displaying morphological traits that did not differ significantly from controls. The subtle variations, observed in the average neurite length and thickness, do not account for a significant and consistent impairment in neurite formation during neuroblast development of FX-hESC lines. Although at this stage *FMR1* is already down-regulated in FX cells, it is not completely inactivated. These results are in contrast to the studies performed in *FMR1* KO animals demonstrating shorter and thicker dendritic spines in FX neurites (Bianco et al., 2010; Comery et al., 1997; Guo et al., 2011a; Irwin et al., 2000; Morales et al., 2002; Nimchinsky et al., 2001). However, these alterations are probably due to the lack of FMRP in KO animals at every neuro-developmental stage, resulting in a phenotype that is much more detrimental than that of human FXS individuals that express FMRP at early stages of neurogenesis. Furthermore, studies performed on FX human neural progenitor cells (FX-hNPCs), have shown contradicting results: a decrease in FX-neurite length in one study (Castren et al., 2005), and no differences in neurite morphology between FX and controls, in another study (Bhattacharyya et al., 2008). Irwin et al. (2000, 2001) have shown that in adult FX human brain samples, dendritic spines display abnormal morphology. However, this is probably due to the effects FMRP absence in adult neural stem cells (Luo et al., 2010), rather than abnormal development during the embryonic period. Altogether, these results suggest that in human, FMRP role in neurite formation is probably less critical than that observed in KO animal models.

At late stages of neurogenesis we demonstrated low neurogenic potential of FX-hESC lines, concomitant with absence of FMRP in FX neurons expressing MAP2 and NeuN. In the same cultures, FX lines showed a strong bias towards differentiation into GFAP expressing cells. These GFAP positive cells still express FMRP, albeit originating from the same full mutated FX-hESC lines. This can be explained either by a higher gliogenic potential of the FX lines, or by impaired maturation, which prevents NPCs expressing GFAP to mature into neurons (Guo et al., 2011a; Kazanis and ffrench-Constant, 2011). A same GFAP bias was observed during neurogenesis of fetal FX-hNPCs, *fmr1*$^{-/-}$ murine adult and embryonic neural stem cells, as well as in FX-hiPSCs (Castren, 2006; Castren et al., 2005; Luo et al., 2010; Sheridan et al., 2011). However, the FX-hESCs model is the only one able to show that although FMRP is inactive in neurons (i.e., MAP2$^{+}$, NeuN$^{+}$) GFAP$^{+}$ cells still express FMRP. Indeed, an active role for FMRP was suggested in the astrocytic lineage (Pacey and Doering, 2007). However, this study also found cells co-expressing GFAP and β-III-Tubulin, interpreted as a mixed subpopulation of uncommitted glial and neural precursors. Similarly, we have also found a subpopulation of cells co-expressing both MAP2 and GFAP, suggesting that, at least in part, the bias towards GFAP over-expression in FX lines represents lack of neural maturity. The low efficiency in MAP2$^{+}$ cells production observed in all three FX lines resembles that of the control HUES-6, which is known to have inherent low neurogenic potential, resulting in both low neural and glial yield (Bock et al., 2011). However, each FX-hESC line was originated from a different unrelated blastocyst. It is possible to conclude that all three lines, independently, are inherently low neurogenic (similar to HUES-6), but this conclusion would not take into account the strong FX-related GFAP-expression bias and the fact that in all three FX lines, MAP2$^{+}$ cells were FMRP$^{-}$, but GFAP$^{+}$ cells were FMRP$^{+}$. Taken together, these data suggest that *FMR1* down-regulation and consequent FMRP absence result in a delayed and reduced maturation of neural precursors into the neuronal lineage. Under in-vitro conditions, this phenomenon leads to an over-expression of GFAP, indicating both a lack of maturation in some of the cells, and a shift in cell fate in others.

The functional analysis of the derived FX neurons demonstrates poor synaptic capability and lack of response to glutamate, despite normal intrinsic properties. The harsh effect of FMRP absence on synaptogenesis or synaptic maintenance could be linked to the in-vitro process that seems to accelerate *FMR1* down-regulation. It is possible that in-vitro down-regulation of *FMR1* during neural differentiation of FX-hESCs is faster than the human in-vivo process. Therefore, it is tempting to speculate that in human FX-fetuses FMRP is completely absent only after the glutamate-dependent synaptic machinery is established. We suggest that in-vitro neural differentiation of FX-hESCs may accelerate the process of *FMR1* down-regulation, causing a grave impairment in synaptogenesis, whereas in-vivo this process is probably slower, resulting in less severe effects. These aspects of correlation between FMRP timing of under-expression and synaptogenesis are hard to study in humans, because of limited biological material (Bhattacharyya et al., 2008; Castren et al., 2005) and the non-dynamic nature of hiPSCs (Urbach et al., 2010). FX-hESCs offer a platform for further understanding of the relationship between FMRP and synaptogenesis. Recently, three studies were published in which FXS was ameliorated, following treatment with metabotropic glutamate receptors antagonists (Michalon et al., 2012; Thomas et al., 2012; Vinueza Veloz et al., 2012). However, in all three studies, the suggested drugs were examined on *fmr1*$^{-/-}$ mouse models. The differences in FX neurogenesis between KO animals and the FX-hESCs shown here, suggest that a well-based human drug-screening model is needed for finding a suitable therapy for the amelioration of early FXS symptoms and the improvement of cognitive functions.

In conclusion, the FX-hESC model can recapitulate in-vitro, many of the pathological events that take place during FXS embryonic and fetal neurogenesis, providing tools for the understanding of aberrant neural differentiation at a molecular level and in a spatiotemporal sequential paradigm. This model enables the tracking of neural impairments associated with the absence of FMRP during all stages of neural differentiation, and may also guide the search for new therapeutic strategies that could counteract inherited FXS related intellectual disability.

## Acknowledgments

The authors thank Prof. Ami Amit, head of the Racine IVF Unit, for provision of IVF and PGD patients. Dr. Rachel Eiges, from Shaare Zedek Medical Center, for providing the FX-hESC line SZFX6 (FX2). Dr. Douglas Melton from Harvard University for providing the different HUES hESC lines used as controls. Dr. Mira Malcov is thanked for performing the PGD analysis of FXS patients and haplotype analysis of FX-hESC lines. Tsvia Frumkin is thanked for karyotype analysis and skillful assistance in the stem cell research lab, and Dr. Yael Kalma for comprehensive reading of the manuscript. The embryologists of the Racine IVF lab, Ariela Carmon, Tanya Cohen, Tamar Shwartz, Nava Mei-Raz and Roee Sela and the molecular biologists, Veronica Gold, Dr. Sagit Peleg and Victoria Lisiansky of the PGD lab in the Sourasky Tel-Aviv Medical Center, for their skillful assistance. The authors thank Tova Neumann for performing FMR1 sizing and Prof. Yuval Yaron, head of the Prenatal Diagnosis Unit, for genetic counseling.

This research was partly funded by a grant from the Chief Scientist Office of the Israel Ministry of Health (300000-6237), by

a grant from the Israel Science Foundation (227/06) and by an Excellency Grant from Tel-Aviv Sourasky Medical Center.

## Appendix A. Supporting information

Supplementary data associated with this article can be found in the online version at http://dx.doi.org/10.1016/j.ydbio.2012.11.031.

## References


Abitbol, M., Menini, C., Delezoide, A.L., Rhyner, T., Vekemans, M., Mallet, J., 1993. Nucleus basalis magnocellularis and hippocampus are the major sites of FMR-1 expression in the human fetal brain. Nat. Genet. 4, 147–153.

Beckel-Mitchener, A., Greenough, W.T., 2004. Correlates across the structural, functional, and molecular phenotypes of fragile X syndrome. Ment. Retard. Dev. Disabil. Res. Rev. 10, 53–59.

Ben-Yosef, D., Amit, A., Malcov, M., Frumkin, T., Ben-Yehudah, A., Eldar, I., Mey-Raz, N., Azem, F., Altarescu, G., Renbaum, P., Beeri, R., Varshaver, I., Eldar-Geva, T., Epsztejn-Litman, S., Levy-Lahad, E., Eiges, R., 2011. Female sex bias in human embryonic stem cell Lines. Stem Cells Dev..

Bhakar, A.L., Dolen, G., Bear, M.F., 2012. The pathophysiology of fragile X (and what it teaches us about synapses). Annu. Rev. Neurosci. 35, 417–443.

Bhattacharyya, A., McMillan, E., Wallace, K., Tubon Jr, T.C., Capowski, E.E., Svendsen, C.N., 2008. Normal neurogenesis but abnormal gene expression in human fragile X cortical progenitor cells. Stem. Cells Dev. 17, 107–117.

Bianco, A., Dienstbier, M., Salter, H.K., Gatto, G., Bullock, S.L., 2010. Bicaudal-D regulates fragile X mental retardation protein levels, motility, and function during neuronal morphogenesis. Curr. Biol. 20, 1487–1492.

Bock, C., Kiskinis, E., Verstappen, G., Gu, H., Boulting, G., Smith, Z.D., Ziller, M., Croft, G.F., Amoroso, M.W., Oakley, D.H., Gnirke, A., Eggan, K., Meissner, A., 2011. Reference maps of human ES and iPS cell variation enable high-throughput characterization of pluripotent cell lines. Cell 144, 439–452.

Borghese, L., Dolezalova, D., Opitz, T., Haupt, S., Leinhaas, A., Steinfarz, B., Koch, P., Edenhofer, F., Hampl, A., Brustle, O., 2010. Inhibition of notch signaling in human embryonic stem cell-derived neural stem cells delays G1/S phase transition and accelerates neuronal differentiation in vitro and in vivo. Stem Cells 28, 955–964.

Braun, K., Segal, M., 2000. FMRP involvement in formation of synapses among cultured hippocampal neurons. Cereb. Cortex 10, 1045–1052.

Castren, M., 2006. Differentiation of neuronal cells in fragile X syndrome. Cell Cycle 5, 1528–1530.

Castren, M., Tervonen, T., Karkkainen, V., Heinonen, S., Castren, E., Larsson, K., Bakker, C.E., Oostra, B.A., Akerman, K., 2005. Altered differentiation of neural stem cells in fragile X syndrome. Proc. Natl. Acad. Sci. USA 102, 17834–17839.

Chambers, S.M., Fasano, C.A., Papapetrou, E.P., Tomishima, M., Sadelain, M., Studer, L., 2009. Highly efficient neural conversion of human ES and iPS cells by dual inhibition of SMAD signaling. Nat. Biotechnol. 27, 275–280.

Chen, Y., Tassone, F., Berman, R.F., Hagerman, P.J., Hagerman, R.J., Willemsen, R., Pessah, I.N., 2010. Murine hippocampal neurons expressing Fmr1 gene pre-mutations show early developmental deficits and late degeneration. Hum. Mol. Genet. 19, 196–208.

Christian, J.L., 2000. BMP, Wnt and Hedgehog signals: how far can they go? Curr. Opin. Cell Biol. 12, 244–249.

Comery, T.A., Harris, J.B., Willems, P.J., Oostra, B.A., Irwin, S.A., Weiler, I.J., Greenough, W.T., 1997. Abnormal dendritic spines in fragile X knockout mice: maturation and pruning deficits. Proc. Natl. Acad. Sci. USA 94, 5401–5404.

Cowan, C.A., Klimanskaya, I., McMahon, J., Atienza, J., Witmyer, J., Zucker, J.P., Wang, S., Morton, C.C., McMahon, A.P., Powers, D., Melton, D.A., 2004. Derivation of embryonic stem-cell lines from human blastocysts. N. Engl. J. Med. 350, 1353–1356.

D'Hulst, C., Kooy, R.F., 2009. Fragile X syndrome: from molecular genetics to therapy. J. Med. Genet. 46, 577–584.

den Broeder, M.J., van der Linde, H., Brouwer, J.R., Oostra, B.A., Willemsen, R., Ketting, R.F., 2009. Generation and characterization of FMR1 knockout zebrafish. PLoS One 4, e7910.

Eiges, R., Urbach, A., Malcov, M., Frumkin, T., Schwartz, T., Amit, A., Yaron, Y., Eden, A., Yanuka, O., Benvenisty, N., Ben-Yosef, D., 2007. Developmental study of fragile X syndrome using human embryonic stem cells derived from preimplantation genetically diagnosed embryos. Cell Stem Cell 1, 568–577.

Frumkin, T., Malcov, M., Telias, M., Gold, V., Schwartz, T., Azem, F., Amit, A., Yaron, Y., Ben-Yosef, D., 2010. Human embryonic stem cells carrying mutations for severe genetic disorders. In Vitro Cell Dev. Biol. Anim.

Georgala, P.A., Carr, C.B., Price, D.J., 2011. The role of Pax6 in forebrain development. Dev. Neurobiol. 71, 690–709.

Guo, W., Allan, A.M., Zong, R., Zhang, L., Johnson, E.B., Schaller, E.G., Murthy, A.C., Goggin, S.L., Eisch, A.J., Oostra, B.A., Nelson, D.L., Jin, P., Zhao, X., 2011a. Ablation of Fmrp in adult neural stem cells disrupts hippocampus-dependent learning. Nat. Med. 17, 559–565.

Guo, W., Murthy, A.C., Zhang, L., Johnson, E.B., Schaller, E.G., Allan, A.M., Zhao, X., 2011b. Inhibition of GSK3beta improves hippocampus-dependent learning and rescues neurogenesis in a mouse model of fragile X syndrome. Hum. Mol. Genet..

Hagerman, P.J., Stafstrom, C.E., 2009. Origins of epilepsy in fragile x syndrome. Epilepsy Curr. 9, 108–112.

Hagerman, R.J., 1987. Fragile-X chromosome and learning disability. J. Am. Acad. Child Adolesc. Psychiatry 26, 938.

Irwin, S.A., Galvez, R., Greenough, W.T., 2000. Dendritic spine structural anomalies in fragile-X mental retardation syndrome. Cereb. Cortex 10, 1038–1044.

Irwin, S.A., Patel, B., Idupulapati, M., Harris, J.B., Crisostomo, R.A., Larsen, B.P., Kooy, F., Willems, P.J., Cras, P., Kozlowski, P.B., Swain, R.A., Weiler, I.J., Greenough, W.T., 2001. Abnormal dendritic spine characteristics in the temporal and visual cortices of patients with fragile-X syndrome: a quantitative examination. Am. J. Med. Genet. 98, 161–167.

Kazanis, I., ffrench-Constant, C., 2011. Extracellular matrix and the neural stem cell niche. Dev. Neurobiol. 71, 1006–1017.

Kormish, J.D., Sinner, D., Zorn, A.M., 2010. Interactions between SOX factors and Wnt/beta-catenin signaling in development and disease. Dev. Dyn. 239, 56–68.

Lim, J.H., Luo, T., Sargent, T.D., Fallon, J.R., 2005. Developmental expression of Xenopus fragile X mental retardation-1 gene. Int. J. Dev. Biol. 49, 981–984.

Luo, Y., Shan, G., Guo, W., Smrt, R.D., Johnson, E.B., Li, X., Pfeiffer, R.L., Szulwach, K.E., Duan, R., Barkho, B.Z., Li, W., Liu, C., Jin, P., Zhao, X., 2010. Fragile x mental retardation protein regulates proliferation and differentiation of adult neural stem/progenitor cells. PLoS Genet. 6, e1000898.

Malcov, M., Naiman, T., Yosef, D.B., Carmon, A., Mey-Raz, N., Amit, A., Vagman, I., Yaron, Y., 2007. Preimplantation genetic diagnosis for fragile X syndrome using multiplex nested PCR. Reprod. Biomed. 14, 515–521. (Online).

Michalon, A., Sidorov, M., Ballard, T.M., Ozmen, L., Spooren, W., Wettstein, J.G., Jaeschke, G., Bear, M.F., Lindemann, L., 2012. Chronic pharmacological mGlu5 inhibition corrects fragile X in adult mice. Neuron 74, 49–56.

Mientjes, E.J., Nieuwenhuizen, I., Kirkpatrick, L., Zu, T., Hoogeveen-Westerveld, M., Severijnen, L., Rife, M., Willemsen, R., Nelson, D.L., Oostra, B.A., 2006. The generation of a conditional Fmr1 knock out mouse model to study Fmrp function in vivo. Neurobiol. Dis. 21, 549–555.

Morales, J., Hiesinger, P.R., Schroeder, A.J., Kume, K., Verstreken, P., Jackson, F.R., Nelson, D.L., Hassan, B.A., 2002. Drosophila fragile X protein, DFXR, regulates neuronal morphology and function in the brain. Neuron 34, 961–972.

Nimchinsky, E.A., Oberlander, A.M., Svoboda, K., 2001. Abnormal development of dendritic spines in FMR1 knock-out mice. J. Neurosci. 21, 5139–5146.

Osafune, K., Caron, L., Borowiak, M., Martinez, R.J., Fitz-Gerald, C.S., Sato, Y., Cowan, C.A., Chien, K.R., Melton, D.A., 2008. Marked differences in differentiation propensity among human embryonic stem cell lines. Nat. Biotechnol. 26, 313–315.

Pacey, L.K., Doering, L.C., 2007. Developmental expression of FMRP in the astrocyte lineage: implications for fragile X syndrome. Glia 55, 1601–1609.

Patapoutian, A., Reichardt, L.F., 2000. Roles of Wnt proteins in neural development and maintenance. Curr. Opin. Neurobiol. 10, 392–399.

Penagarikano, O., Mulle, J.G., Warren, S.T., 2007. The pathophysiology of fragile X syndrome. Annu. Rev. Genomics Hum. Genet. 8, 109–129.

Reubinoff, B.E., Pera, M.F., Fong, C.Y., Trounson, A., Bongso, A., 2000. Embryonic stem cell lines from human blastocysts: somatic differentiation in vitro. Nat. Biotechnol. 18, 399–404.

Schwartz, P.H., Tassone, F., Greco, C.M., Nethercott, H.E., Ziaeian, B., Hagerman, R.J., Hagerman, P.J., 2005. Neural progenitor cells from an adult patient with fragile X syndrome. BMC Med. Genet. 6, 2.

Sheridan, S.D., Theriault, K.M., Reis, S.A., Zhou, F., Madison, J.M., Daheron, L., Loring, J.F., Haggarty, S.J., 2011. Epigenetic characterization of the FMR1 gene and aberrant neurodevelopment in human induced pluripotent stem cell models of fragile X syndrome. PLoS One 6, e26203.

Shih, Y.H., Kuo, C.L., Hirst, C.S., Dee, C.T., Liu, Y.R., Laghari, Z.A., Scotting, P.J., 2010. SoxB1 transcription factors restrict organizer gene expression by repressing multiple events downstream of Wnt signalling. Development 137, 2671–2681.

Sutcliffe, J.S., Nelson, D.L., Zhang, F., Pieretti, M., Caskey, C.T., Saxe, D., Warren, S.T., 1992. DNA methylation represses FMR-1 transcription in fragile X syndrome. Hum. Mol. Genet. 1, 397–400.

Thomas, A.M., Bui, N., Perkins, J.R., Yuva-Paylor, L.A., Paylor, R., 2012. Group I metabotropic glutamate receptor antagonists alter select behaviors in a mouse model for fragile X syndrome. Psychopharmacology (Berl) 219, 47–58.

Thomson, J.A., Itskovitz-Eldor, J., Shapiro, S.S., Waknitz, M.A., Swiergiel, J.J., Marshall, V.S., Jones, J.M., 1998. Embryonic stem cell lines derived from human blastocysts. Science 282, 1145–1147.

Urbach, A., Bar-Nur, O., Daley, G.Q., Benvenisty, N., 2010. Differential modeling of fragile X syndrome by human embryonic stem cells and induced pluripotent stem cells. Cell Stem Cell 6, 407–411.

Verkerk, A.J., Pieretti, M., Sutcliffe, J.S., Fu, Y.H., Kuhl, D.P., Pizzuti, A., Reiner, O., Richards, S., Victoria, M.F., Zhang, F.P., et al., 1991. Identification of a gene (FMR-1) containing a CGG repeat coincident with a breakpoint cluster region exhibiting length variation in fragile X syndrome. Cell 65, 905–914.

Vinueza Veloz, M.F., Buijsen, R.A., Willemsen, R., Cupido, A., Bosman, L.W., Koekkoek, S.K., Potters, J.W., Oostra, B.A., De Zeeuw, C.I., 2012. The effect of an mGluR5 inhibitor on procedural memory and avoidance discrimination impairments in Fmr1 KO mice. Genes Brain Behav. 11, 325–331.

Wan, L., Dockendorff, T.C., Jongens, T.A., Dreyfuss, G., 2000. Characterization of dFMR1, a Drosophila melanogaster homolog of the fragile X mental retardation protein. Mol. Cell Biol. 20, 8536–8547.
Wang, T., Bray, S.M., Warren, S.T., 2012. New perspectives on the biology of fragile X syndrome. Curr. Opin. Genet. Dev. 22, 256–263.
Willemsen, R., Bontekoe, C.J., Severijnen, L.A., Oostra, B.A., 2002. Timing of the absence of FMR1 expression in full mutation chorionic villi. Hum. Genet 110, 601–605.
Willemsen, R., Oostra, B.A., Bassell, G.J., Dictenberg, J., 2004. The fragile X syndrome: from molecular genetics to neurobiology. Ment. Retard. Dev. Disabil. Res. Rev. 10, 60–67.
Wilson, P.G., Stice, S.S., 2006. Development and differentiation of neural rosettes derived from human embryonic stem cells. Stem Cell Rev. 2, 67–77.
Xia, X., Zhang, S.C., 2009. Differentiation of neuroepithelia from human embryonic stem cells. Methods Mol. Biol. 549, 51–58.
Yan, B., Neilson, K.M., Moody, S.A., 2009. Notch signaling downstream of foxD5 promotes neural ectodermal transcription factors that inhibit neural differentiation. Dev. Dyn. 238, 1358–1365.
Zhang, X.Q., Zhang, S.C., 2010. Differentiation of neural precursors and dopaminergic neurons from human embryonic stem cells. Methods Mol. Biol. 584, 355–366.